Check for updates

Accepted Article

A Biomimetic Nociceptor Using Centrosymmetric Crystals for Machine Intelligence

Wenjie Wang, Yingfei Wang, Li Xiang, Long Chen, Lilei Yu, Anlian Pan, Jie Tan, and Quan Yuan**

W. Wang, Y. Wang, L. Xiang, A. Pan, J. Tan, Q. Yuan

Molecular Science and Biomedicine Laboratory (MBL), State Key Laboratory of Chemo/Biosensing and Chemometrics, Key Laboratory for Micro-Nano Physics and Technology of Hunan Province, College of Chemistry and Chemical Engineering, College of Materials Science and Engineering, Hunan University, Changsha 410082, China

E-mail: yuanquan@whu.edu.cn; tanjie0416@hnu.edu.cn

ORCID: 0000-0002-3085-431X (Quan Yuan); 0000-0002-0909-2904 (Jie Tan)

L. Chen

This article has been accepted for publication and undergone full peer review but has not been through the copyediting, typesetting, pagination and proofreading process, which may lead to differences between this version and the Version of Record. Please cite this article as doi: 10.1002/adma.202310555.

This article is protected by copyright. All rights reserved.

Accepted Article

Department of Computer and Information Science, Faculty of Science and Technology, University of Macau, Macau SAR, China

L. Yu, Q. Yuan

College of Chemistry and Molecular Sciences, Department of Cardiology, Institute of Molecular Medicine, Renmin Hospital of Wuhan University, Wuhan University, Wuhan 430072, China

Keywords: biomimetic nociceptors, multimodal sensors, triboelectric effect, intelligent terminals, mechanoluminescence

Pain sensation is a crucial aspect of perception in the body. Force-activated nociceptors encode electrochemical signals and yield multilevel information of pain, thus enabling smart feedback. Inspired by the natural template, multi-dimensional mechano-sensing materials provide promising approaches for biomimetic nociceptors in intelligent terminals. However, the reliance on non-centrosymmetric crystals has narrowed the range of these materials. Here we report centrosymmetric crystal Cr^{3+}-doped zinc gallogermanate (ZGGO:Cr) with multi-dimensional mechano-sensing, eliminating the limitation of crystal structure. Under forces, ZGGO:Cr generates electrical signals imitating those of neuronal systems, and produces luminescence for spatial mapping of mechanical stimuli, suggesting a path toward bionic pain perception. On that basis, we developed a

This article is protected by copyright. All rights reserved.

15214095, ja, Downloaded from https://onlinelibrary.wiley.com/doi/10.1002/adma.202310555 by Wuhan University, Wiley Online Library on [01/12/2023]. See the Terms and Conditions (https://onlinelibrary.wiley.com/terms-and-conditions) on Wiley Online Library for rules of use; OA articles are governed by the applicable Creative Commons License

wireless biomimetic nociceptor system and achieved a smart pain reflex in a robotic hand and robot-assisted biopsy surgery of rat and dog.

1. Introduction

Pain sensation is one of the body's crucial aspects of perception.[1] The 2021 Nobel Prize in Physiology or Medicine accentuated the importance of the molecular basis of pain.[2] The perceptions of pain convey valuable information about the environment to elicit a proper body response and avoid potential damage.[3] Specifically, free nerve endings in the epidermis act as nociceptors and respond to noxious stimuli through Aβ, Aδ and C nerve fibers, activating the corresponding brain regions, resulting in pain perception and producing feedback.[1, 3] During this process, the electrical signal produced by nerve fibers is a measure of stimulus magnitude, while activation of the brain cortex can track the spatial locations of noxious stimuli by activating different parts of the body map.[4]

As a natural template for intelligent terminals, pain perception can be reproduced via electrical and optical signals to imitate, respectively, the neuronal current signal and spatial mapping of a mechanical stimulus.[5] Intelligent analysis algorithms will help replicate the brain features of multimodal and intelligent recognition of pain to support pain perception, location and feedback in intelligent terminals.[6] Nature has evolved nociceptors as the most

This article is protected by copyright. All rights reserved.

Accepted Article

15214095, ja, Downloaded from https://onlinelibrary.wiley.com/doi/10.1002/adma.202310555 by Wuhan University, Wiley Online Library on [01/12/2023]. See the Terms and Conditions (https://onlinelibrary.wiley.com/terms-and-conditions) on Wiley Online Library for rules of use; OA articles are governed by the applicable Creative Commons License

Accepted Article

rational means to encode mechanical stimuli into physiological signals that can be interpreted by the brain.[7] By mimicking nociceptors in a single unit, the realization of mechano-sensing with optical and electrical dual response can facilitate further algorithm analysis and integration of device.[8] A prerequisite for such a unit is development of materials that produce force-dependent optical signals and electrical signals.[8b, 9]

The conventional mechano-responsive materials usually consist of crystalline materials exhibiting both piezoelectric and mechanoluminescent effects.[10] The materials deform along the direction of an applied force, resulting in separation of charge centers and an electric field. The electrons may be transmitted to a luminescent center and generate photon emission.[10a, 11] As a premise, these materials must have non-centrosymmetric crystal structures.[12] However, the limited scope of non-centrosymmetric compounds has remained a major obstacle for design of mechano-sensing materials.[13] In this context, materials that exhibit the triboelectric effect can produce charges on a material surface upon mechanical stimuli, thus providing a possible pathway for centrosymmetric crystals to realize mechano-sensing, circumventing the reliance on crystal structure.[14]

Here, we report centrosymmetric Cr^{3+}-doped zinc gallogermanate (denoted as ZGGO:Cr) as a multi-dimensional mechano-sensing “nociceptor”. Under an applied force, the

This article is protected by copyright. All rights reserved.

15214095, ja, Downloaded from https://onlinelibrary.wiley.com/doi/10.1002/adma.202310555 by Wuhan University, Wiley Online Library on [01/12/2023]. See the Terms and Conditions (https://onlinelibrary.wiley.com/terms-and-conditions) on Wiley Online Library for rules of use; OA articles are governed by the applicable Creative Commons License

Accepted Article

triboelectricity causes the energy bands of ZGGO:Cr to tilt, so that pre-filled electrons in traps can transfer to a luminescent centers to produce luminescence.[15] We used ZGGO:Cr as the basis for a biomimetic nociceptor, with electrical signals quantitatively evaluating the amplitude of the force (pain level) and the visual luminescence output providing spatial mapping of force, thus closely mimicking a pain perception system (**Figure 1**). A machine-learning algorithm was implemented to decode the electrical and optical output signals for intelligent pain reflex. An interactive program and wireless module were further integrated as feedback components of the biomimetic nociceptor, realizing stimuli-activated reflex movements of a robotic hand. In addition, this biomimetic nociceptor was implemented in a surgical robot to assist the surgeon in decisions and improve surgical safety. Taken together, this wireless biomimetic nociceptor offers a strategy to accurately evaluate external stimuli and elicit appropriate responses, thus shaping the next generation of intelligent terminals and robotic technologies.

This article is protected by copyright. All rights reserved.

15214095, ja, Downloaded from https://onlinelibrary.wiley.com/doi/10.1002/adma.202310555 by Wuhan University, Wiley Online Library on [01/12/2023]. See the Terms and Conditions (https://onlinelibrary.wiley.com/terms-and-conditions) on Wiley Online Library for rules of use; OA articles are governed by the applicable Creative Commons License

Accepted Article

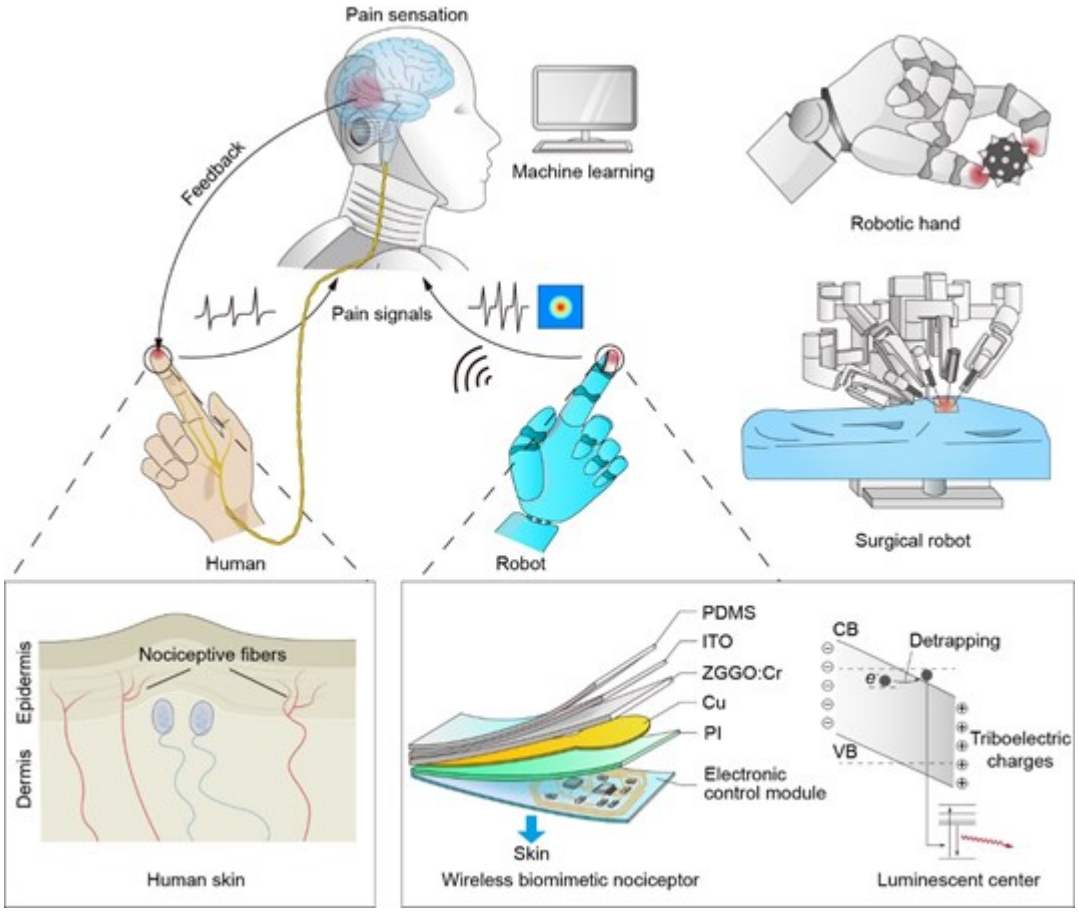

Figure 1. Biomimetic nociceptor mimicking the biological system and its application in intelligent terminals. The body pain perception detects and localizes harmful stimuli via free nerve endings in the epidermis (nociceptor). Via the central nervous system, these are transmitted to the corresponding regions of brain, where they are decoded, and provide sensory feedback. The biomimetic nociceptor system mimics this process by using force-induced current and mechanoluminescence in ZGGO:Cr to quantify and track

This article is protected by copyright. All rights reserved.

15214095, ja, Downloaded from https://onlinelibrary.wiley.com/doi/10.1002/adma.202310555 by Wuhan University, Wiley Online Library on [01/12/2023]. See the Terms and Conditions (https://onlinelibrary.wiley.com/terms-and-conditions) on Wiley Online Library for rules of use; OA articles are governed by the applicable Creative Commons License

Accepted Article

mechanical stimuli, respectively. The responses activate a machine learning-based algorithm to interpret the multimodal signals from ZGGO:Cr. On this basis, intelligent terminals (e.g., robotic hand and surgical robot) can be created with human-like pain reflexes and feedback.

2. Results

2.1. Preparation and mechanical responsiveness of ZGGO:Cr

Mechanical force-induced neuronal current and projections to cortical areas, as well as decoding of multimodal information within the brain, are especially critical in pain evaluation, location and feedback in pain perception.[16] To create a biomimetic nociceptor device, it is highly desirable to develop materials that can convert mechanical energy into both light energy and electrical energy for spatial mapping and quantification of force.[6a, 17] The optical and electrical signals are functionally similar to the pulse-like stimulation in brain cortex and nerve tissue, respectively, for conversion of external mechanical stimuli into readable and processable information.[7c, 7d] Furthermore, the interrelated optical and electrical signals can provide multi-dimensional information, ideally mimicking the human pain reflex, for intuitive interactions of smart devices.

This article is protected by copyright. All rights reserved.

15214095, ja, Downloaded from https://onlinelibrary.wiley.com/doi/10.1002/adma.202310555 by Wuhan University, Wiley Online Library on [01/12/2023]. See the Terms and Conditions (https://onlinelibrary.wiley.com/terms-and-conditions) on Wiley Online Library for rules of use; OA articles are governed by the applicable Creative Commons License

Accepted Article

Herein we introduce centrosymmetric material ZGGO:Cr as a mechano-sensing material with optical and electrical dual response for a biomimetic nociceptor. The crystal structure of ZGGO:Cr is shown in **Figure 2a**. According to the crystal data (**Figure S1**), ZGGO:Cr belongs to the cubic space group F3dm, in which Zn^{2+} and Ga^{3+} exist in the forms of [ZnO_4] tetrahedra and [GaO_8] octahedra, respectively.[18] Considering the ionic radii and coordination numbers (CN), Ga^{3+} (0.62 Å, CN=6), Cr^{3+} (0.615 Å, CN=6) and Ge^{4+} (0.53 Å, CN=6), the dopants Cr^{3+} and Ge^{4+} should substitute at the Ga^{3+} site in ZGGO:Cr to form a solid solution.[19] The formation of anti-site defects (Zn and Ga at exchanged positions) was found to be energetically favored.[20] We fabricated a sandwiched sensing unit with a mechano-sensitive component (ZGGO:Cr powders) inserted it between two electrodes (Cu and Al) with large surface potential differences .The optical and electrical signals obtained under various applied pressures were recorded with a charge-coupled device (CCD) camera and electrochemical workstation, respectively (**Figure 2b**). Our result demonstrated that the mechanoluminescence intensity of ZGGO:Cr strongly depends on the applied mechanical force (**Figure 2c,d**). In addition, an increase in mechanical force resulted in an increase in voltage output (**Figure 2e**). After quantitatively analyzing the optical and electrical signals, it was found that these signals of ZGGO:Cr both respond sensitively to mechanical force (**Figure 2f**). These results indicated that ZGGO:Cr is capable of simultaneously converting

This article is protected by copyright. All rights reserved.

15214095, ja, Downloaded from https://onlinelibrary.wiley.com/doi/10.1002/adma.202310555 by Wuhan University, Wiley Online Library on [01/12/2023]. See the Terms and Conditions (https://onlinelibrary.wiley.com/terms-and-conditions) on Wiley Online Library for rules of use; OA articles are governed by the applicable Creative Commons License

mechanical stimuli into optical and electrical signals, which is promising for the realization of pain-related biomimetic neuronal current and projections to cortical areas.

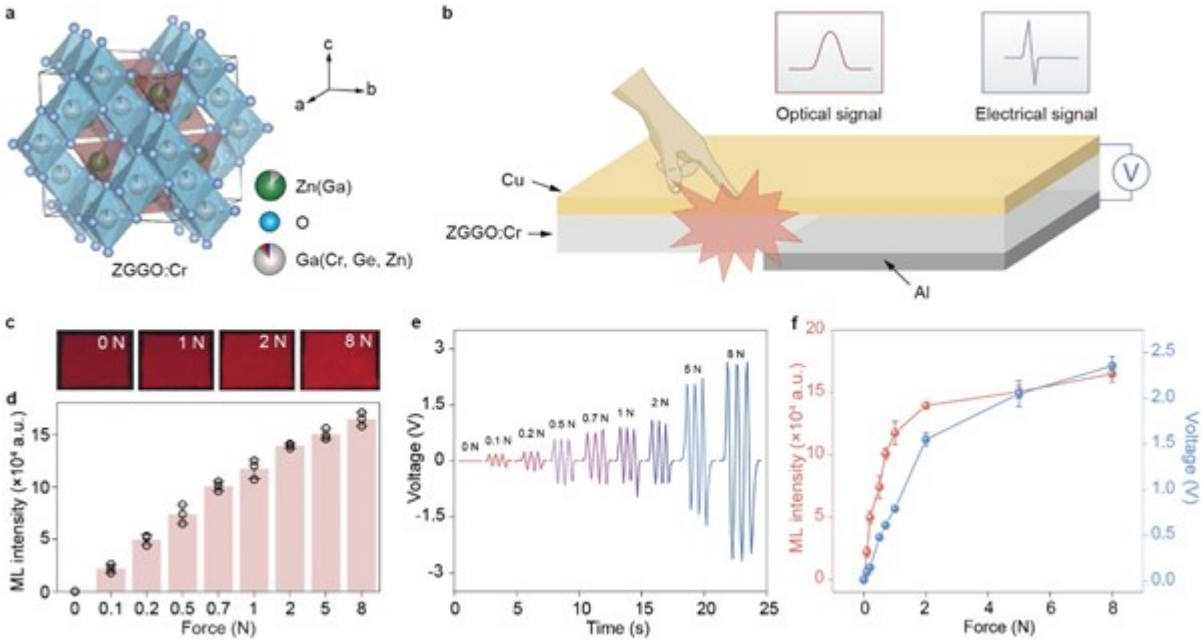

Figure 2. Optical and electrical dual responses in ZGGO:Cr. a) Crystal structure of ZGGO:Cr of the F3dm space group, showing the [ZnO_4] tetrahedra and [GaO_6] octahedra. b) Schematic illustration of the optical and electrical signal analysis in a sandwich-structured sensing unit under forces (not to scale). c) Photographs of mechanoluminescence (ML) images of ZGGO:Cr. d) Dependence of mechanoluminescence intensity on applied force. Data are

This article is protected by copyright. All rights reserved.

Accepted Article

15214095, ja, Downloaded from https://onlinelibrary.wiley.com/doi/10.1002/adma.202310555 by Wuhan University, Wiley Online Library on [01/12/2023]. See the Terms and Conditions (https://onlinelibrary.wiley.com/terms-and-conditions) on Wiley Online Library for rules of use; OA articles are governed by the applicable Creative Commons License

mean ± s.d. n = 3. e) Voltage plots in response to increased force. f) Mechanoluminescence intensity (red) and voltage output (blue) with increased force. Data are mean ± s.d. n = 3.

2.2. Fabrication and characterization of biomimetic nociceptor

Composite films were fabricated by dispersing ZGGO:Cr powders in polydimethylsiloxane (PDMS) (**Figure S2**). **Figure S3** shows the stress-strain curve of the ZGGO:Cr@PDMS composite film, which has a tensile strength of ~0.8 MPa and an elastic modulus of ~1.5 MPa. The biomimetic nociceptor was designed using ZGGO:Cr@PDMS composite film as the sensing element (**Figure S4, S5**, **Movie S1**). **Figure 3a** and **Figure 3b** shows fabrication and an optical image of the wireless biomimetic nociceptor, respectively. The device consists of four layers: Cu film as working electrode, ZGGO:Cr@PDMS film as sensing unit, transparent ITO film as counter electrode, and an electronic control module for signal processing, wireless data transmission and power supply (**Figure S6**). The cross-section scanning electron microscopy (SEM) images show the sandwich structure of the biomimetic nociceptor (**Figure S7**). To intuitively demonstrate the mechanoluminescence performance, the whole mechanoluminescence process was triggered on device while recording a video (**Movie S2**, **Figure S8**). By further analyzing mechanoluminescence

This article is protected by copyright. All rights reserved.

Accepted Article

15214095, ja, Downloaded from https://onlinelibrary.wiley.com/doi/10.1002/adma.202310555 by Wuhan University, Wiley Online Library on [01/12/2023]. See the Terms and Conditions (https://onlinelibrary.wiley.com/terms-and-conditions) on Wiley Online Library for rules of use; OA articles are governed by the applicable Creative Commons License

Accepted Article

intensity, the spatial distribution of applied force can be readily acquired. Next, mechano-sensing with electrical response in the biomimetic nociceptor was investigated. **Figure 3c** and **Figure 3d** plot the triboelectric voltage and current responses of the biomimetic nociceptor. When pressure was applied in the z direction, positive voltage and current output were obtained with increasing pressure, and negative output was acquired with decreasing pressure, illustrating the direct conversion of mechanical energy into electricity. Current output of the biomimetic nociceptor increased with the magnitude of applied pressure: the measured current increased from ~2 nA to ~150 nA in response to an increasing applied pressure in the range of 0.05-5 kPa, with a sensitivity of ~28 $nA \cdot kPa^{-1}$ (**Figure 3e,f**). The output currents were linearly proportional to the applied pressure. The biomimetic nociceptor exhibited excellent flexibility and durability with the same amount of mechanical load after 3000 cycles (**Figure 3g**). It also maintains stable performance in a wide range of daily environments, such as different temperatures and bending (**Figure S9-S16**).

The spatial resolution of pressure distributions was performed on our device with the same magnitude of pressure. The measured current data in different areas showed excellent agreement, and multilocation of mechanoluminescence could be observed depending on pressure location, hence realizing quantification and spatial mapping of pressures

This article is protected by copyright. All rights reserved.

15214095, ja, Downloaded from https://onlinelibrary.wiley.com/doi/10.1002/adma.202310555 by Wuhan University, Wiley Online Library on [01/12/2023]. See the Terms and Conditions (https://onlinelibrary.wiley.com/terms-and-conditions) on Wiley Online Library for rules of use; OA articles are governed by the applicable Creative Commons License

Accepted Article

simultaneously (**Figure 3h**, **Figure S17-S19**). The biomimetic nociceptor exhibited the current change in different fashions for various objects, including brush, cotton swab and needle, thus allowing differentiation between various mechanical stimuli (**Figure 3i-k**, **Figure S20-S22**). Combining the results above, the as-developed biomimetic nociceptor provides reliable performance in multi-dimensional mechano-sensing, offering a route for precise evaluation and visualization of mechanical stimuli and opening opportunities to pain perception.

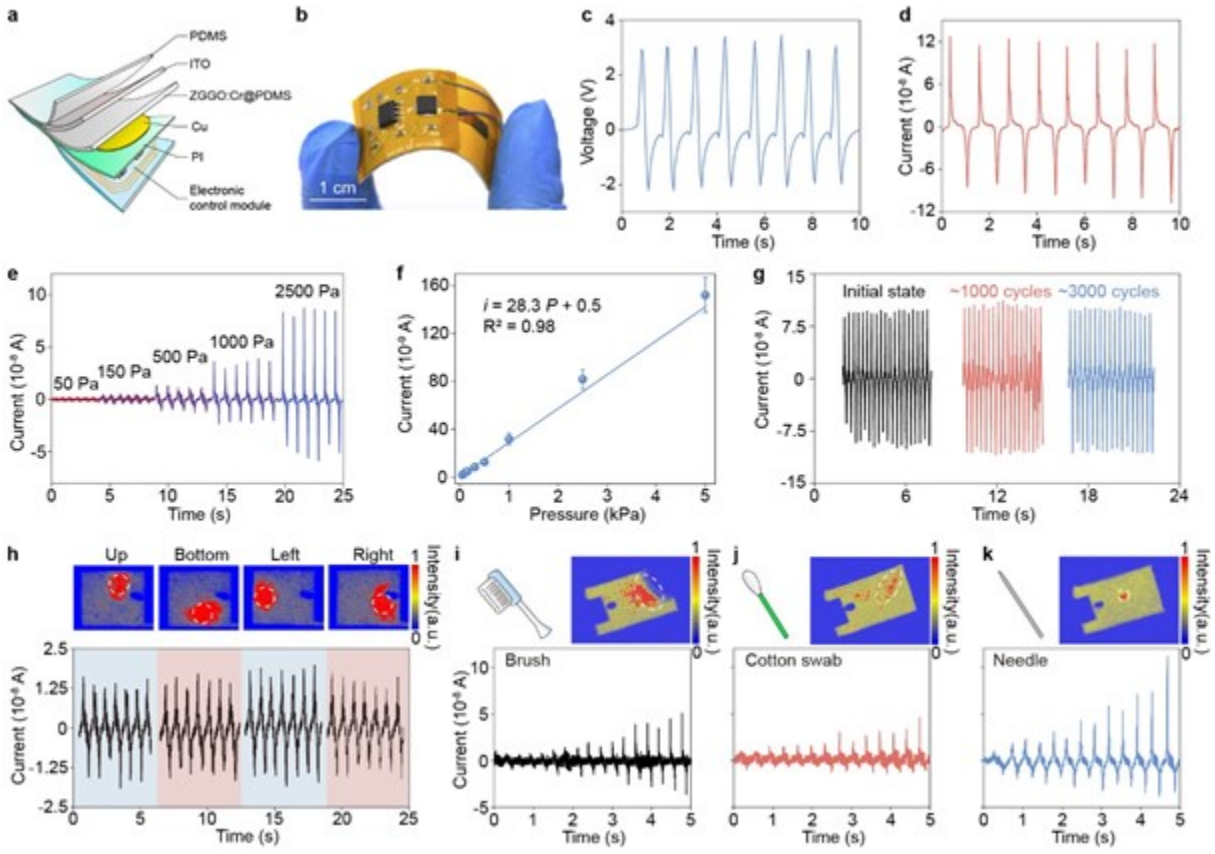

This article is protected by copyright. All rights reserved.

15214095, ja, Downloaded from https://onlinelibrary.wiley.com/doi/10.1002/adma.202310555 by Wuhan University, Wiley Online Library on [01/12/2023]. See the Terms and Conditions (https://onlinelibrary.wiley.com/terms-and-conditions) on Wiley Online Library for rules of use; OA articles are governed by the applicable Creative Commons License

Accepted Article

Figure 3. Characterization of biomimetic nociceptor. a) Device structure of the wireless biomimetic nociceptor. b) Photographic image showing the biomimetic nociceptor that integrates with the electronic control module. c-d) Output voltage signals (c) and output current signals (d) of the device. e) Output current signals of the device under different pressures. f) Peak generated current (I) as a function of applied pressure (P). Data are mean ± s.d. n = 5. g) Endurance test of the device under continuous operation for 1000 and 3000 cycles. h) Mechanoluminescence images (top) and current signals (bottom) recorded by applying forces on different locations across the device. i-k) Mechanoluminescence images (top) and current signals (bottom) caused by brush (i), cotton swab (j) and needle (k) stimuli. The scale bar represents relative luminescence intensity.

2.3. Human pain studies using biomimetic nociceptor

The device can be conformally mounted on the curved surface of the skin via a dual-sided adhesive to support evaluations of pain threshold in the human body (**Figure 4a**). Innocuous stimuli change to intensely painful stimuli under inflammatory conditions.[21] Consistent with a role in nociception, transient receptor potential vanilloid 1 (TRPV1) can be activated by inflammation and can allow extracellular calcium influx through the plasma

This article is protected by copyright. All rights reserved.

15214095, ja, Downloaded from https://onlinelibrary.wiley.com/doi/10.1002/adma.202310555 by Wuhan University, Wiley Online Library on [01/12/2023]. See the Terms and Conditions (https://onlinelibrary.wiley.com/terms-and-conditions) on Wiley Online Library for rules of use; OA articles are governed by the applicable Creative Commons License

Accepted Article

membrane.[22] Capsaicin can activate the nociceptor-specific TRPV1 and induce local inflammation, thus causing sensitization to peripheral stimuli.[23] We applied heat and capsaicin to the forearm and thus lowered the local pain threshold (**Figure S23-S25**). Elevated levels of intracellular calcium were confirmed by aptamers targeting Ca^{2+}, hence indicating capsaicin-induced pain hypersensitivity (**Figure S26, S27**). The device was then mounted on treated area, and mechanical stimuli like brush stroke were exerted with increasing force across skin and the device until the participants reported discomfort or pain sensation. The stimuli-induced electrical current of device at this time was recorded as pain threshold. The biomimetic nociceptor on the forearm revealed a reduction in pain threshold that matched well with local temperature elevation (**Figure 4b**). The pain threshold variation was also measured using von Frey filaments, and the results were quantitatively consistent with measurements using the biomimetic nociceptor (**Figure S28**).

Upon various mechanical stimuli, including brush, cotton swab and finger (**Figure S29**), the mechanoluminescence produced by our device was focused substantially on the areas where the stimuli were applied (**Figure 4c**). The current output reveals the marked drop in pain threshold elicited by various stimuli and the gradual recovery of normal sensation thereafter, in agreement with the von Frey test (**Figure 4d** and **Figure S30**). Pain evoked by a

This article is protected by copyright. All rights reserved.

15214095, ja, Downloaded from https://onlinelibrary.wiley.com/doi/10.1002/adma.202310555 by Wuhan University, Wiley Online Library on [01/12/2023]. See the Terms and Conditions (https://onlinelibrary.wiley.com/terms-and-conditions) on Wiley Online Library for rules of use; OA articles are governed by the applicable Creative Commons License

finger exhibits the fastest recovery from pain hypersensitivity, and has a much higher threshold compared to brush and cotton swab stroke. Of note, this finding shows parallels with the mechanism of pain conduction, where brush- and cotton swab-evoked pain is generally accepted to be mediated by low-threshold Aβ fibers and touch-evoked pain is partially mediated by high-threshold C fibers.[23-24] On the other hand, sensory deficits (such as hypoalgesia) can give rise to diminished ability to perceive painful stimuli and a higher pain threshold.[25] Pain threshold variation under hypoalgesia was assessed with the biomimetic nociceptor, and the results showed the same trend as the von Frey test and visual analog scale (VAS) pain scores (**Figure S31-S37**). Together, these data indicated that the wireless biomimetic nociceptor evaluates the shifts in pain threshold precisely under pain hypersensitivity or sensory deficit.

Accepted Article

This article is protected by copyright. All rights reserved.

15214095, ja, Downloaded from https://onlinelibrary.wiley.com/doi/10.1002/adma.202310555 by Wuhan University, Wiley Online Library on [01/12/2023]. See the Terms and Conditions (https://onlinelibrary.wiley.com/terms-and-conditions) on Wiley Online Library for rules of use; OA articles are governed by the applicable Creative Commons License

Accepted Article

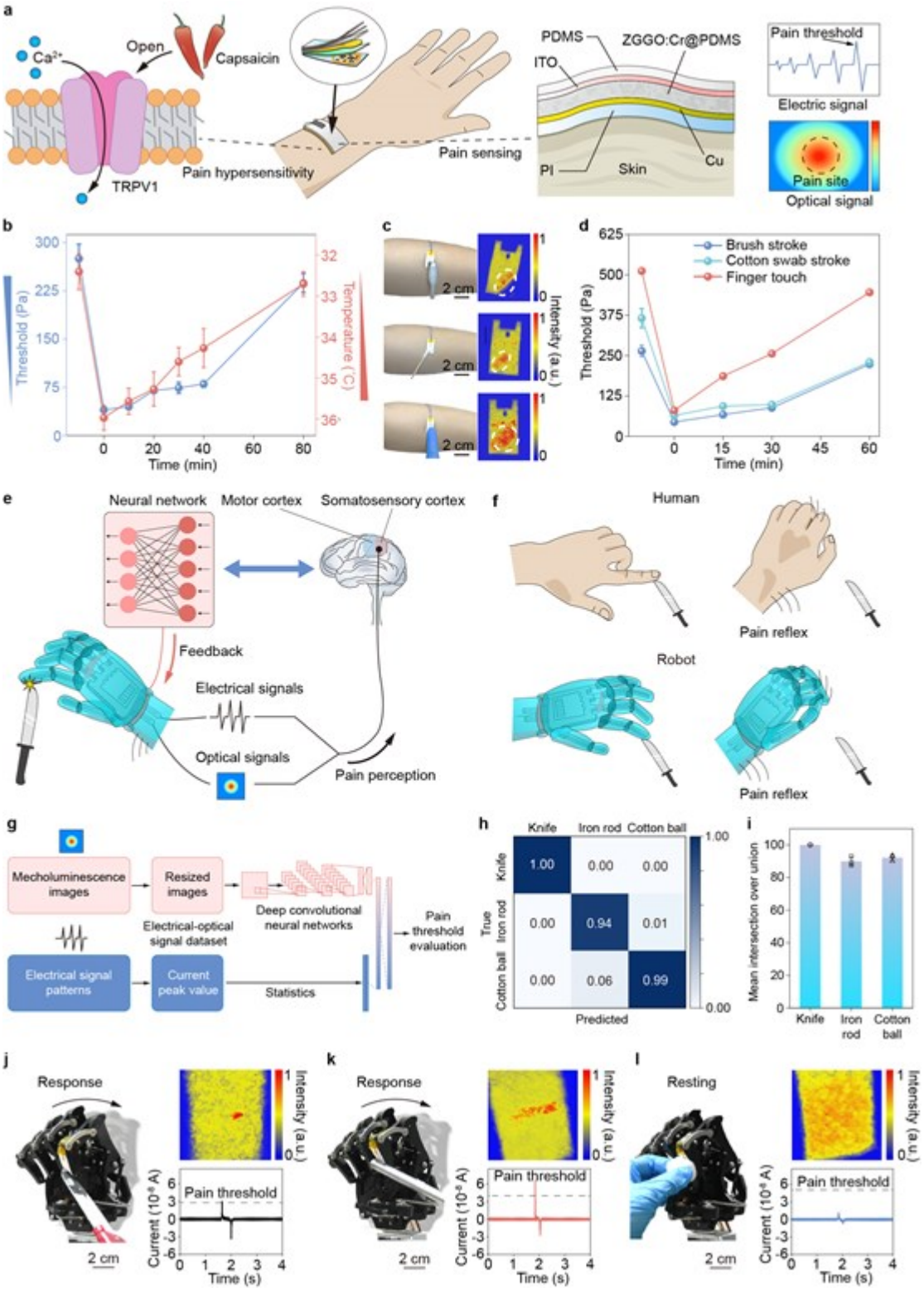

This article is protected by copyright. All rights reserved.

15214095, ja, Downloaded from https://onlinelibrary.wiley.com/doi/10.1002/adma.202310555 by Wuhan University, Wiley Online Library on [01/12/2023]. See the Terms and Conditions (https://onlinelibrary.wiley.com/terms-and-conditions) on Wiley Online Library for rules of use; OA articles are governed by the applicable Creative Commons License

Accepted Article

Figure 4. Demonstration of pain evaluation in the body and pain reflex in the robotic hand. a) Schematic illustration of capsaicin-induced pain hypersensitivity and evaluation using biomimetic nociceptor (not to scale). The TRPV1 receptor is activated by capsaicin, allowing extracellular calcium influx through the plasma membrane and development of pain hypersensitivity. The device is then mounted on the treated area to quantify and map the mechanical-stimuli-evoked pain by electrical and optical signals. b) Variation in pain threshold for brush (blue) and local temperature (red) over time after heat and capsaicin treatment. Data are mean ± s.d. n = 3. c) Photographs and mechanoluminescence images displaying the assessment and localization of pain elicited by various stimuli. Scale bar represents relative luminescence intensity. d) Variation in pain threshold for brush stroke, cotton swab stroke and finger touch over time after heat and capsaicin treatment. Data are mean ± s.d. n = 3. e) Schematic showing that the machine learning algorithms are helping robots decode electrical and optical signals to augment pain sensing and pain reflex, closely mimicking the decoding of multimodal nociceptive information in the human brain (somatosensory cortex) and feedback of the body (motor cortex). f) Sketch depicting the pain reflex in the body and in robotic hand, respectively. g) Diagram demonstrating data collection and processing of electrical and optical signals by deep learning architecture. h) Object classification accuracy after combining electrical and optical signals using deep learning algorithm. i) Comparison of

This article is protected by copyright. All rights reserved.

15214095, ja, Downloaded from https://onlinelibrary.wiley.com/doi/10.1002/adma.202310555 by Wuhan University, Wiley Online Library on [01/12/2023]. See the Terms and Conditions (https://onlinelibrary.wiley.com/terms-and-conditions) on Wiley Online Library for rules of use; OA articles are governed by the applicable Creative Commons License

Accepted Article

the classification results on the test set. Data are mean ± s.d. n = 3. j-l) Left: the robotic hand touching knife (j), iron rod (k) or cotton ball (l). Right: the corresponding mechanoluminescence signals and current signals generated during the manipulations. The scale bar represents relative luminescence intensity. Black dashed lines represent the preset pain threshold for different stimuli.

2.4. Pain reflex performances in robotic hand

The key advantage of body pain perception lies in enabling multilevel information acquisition that helps to interact with the surroundings precisely, rapidly, and safely. For instance, visual sensation, tactile sensation and psychology are all involved in both sensory-discriminative and emotional-affective aspects of pain by activating the network of brain regions such as the prefrontal cortex, anterior cingulate cortex and anterior insula, alerting us to danger and activating suitable reflex movements.[1a] Inspired by this, we investigated the idea that pain sensation could benefit robots by introducing self-preservation and the capability to automatically release objects when pain is perceived. We used our biomimetic nociceptor to mimic human pain reflex that can learn to classify dangerous and safe stimuli by integrating the sensor signals with a deep learning technique (**Figure 4e**).

This article is protected by copyright. All rights reserved.

15214095, ja, Downloaded from https://onlinelibrary.wiley.com/doi/10.1002/adma.202310555 by Wuhan University, Wiley Online Library on [01/12/2023]. See the Terms and Conditions (https://onlinelibrary.wiley.com/terms-and-conditions) on Wiley Online Library for rules of use; OA articles are governed by the applicable Creative Commons License

Accepted Article

Specifically, we acquired a multimodal pain dataset based on electrical and optical signals and used machine learning tools to distil material properties and risk factors from multimodal pain dataset. Then, the algorithm automatically sets the pain threshold value of each object to trigger an intelligent pain reflex (**Figure 4f**). The knife and iron rod were used to elicit different types of noxious mechanical stimuli, and a cotton ball that can be manipulated safely was used to elicit innocuous mechanical stimuli. By using multiple grasps, a custom electrical-optical dataset containing samples consisting of current peak values and mechanoluminescence images was built (**Figure 4g**). We used the dataset and a machine learning technique based on deep convolutional neural networks for object recognition. The final classification performance of the learning strategy was 97.7% after model training (**Figure 4h**).

The data showed that the system reliably classified unknown stimuli as noxious or innocuous stimuli using the learning technique (**Figure 4i**), confirming that the system could perceive stimuli from the learned objects. Based on the material properties identified by the machine learning algorithm, the system automatically set the pain threshold according to the risk factor of objects. As shown in **Movie S3**, the robotic hand had a high likelihood of triggering the withdrawal reflex while touching a knife with sharp edge, but this did not happen

This article is protected by copyright. All rights reserved.

15214095, ja, Downloaded from https://onlinelibrary.wiley.com/doi/10.1002/adma.202310555 by Wuhan University, Wiley Online Library on [01/12/2023]. See the Terms and Conditions (https://onlinelibrary.wiley.com/terms-and-conditions) on Wiley Online Library for rules of use; OA articles are governed by the applicable Creative Commons License

Accepted Article

for the cotton ball (**Figure 4j-l**). Likewise, if the robotic hand grasped the prickly and hard ball with increasing force, the currents grew above the threshold and the robotic hand was informed by the protection program to release the balls. For the soft cotton ball, the robotic hand could manipulate it safely without awakening the protection program (**Movie S4** and **Figure S38, S39**). The results indicated that the biomimetic nociceptor allowed the robotic hand to differentiate innocuous or noxious mechanical stimuli. The robotic hand can also guarantee safe and intelligent interactions with fragile objects (for example, tofu, cake and egg) by precisely setting the current threshold (**Movie S5** and **Figure S40**). Taken together, the dual response pain sensory system and interactive program could provide human-like pain perception to help intelligent terminals perceive and react to external stimuli, determine the pain location, avoid the risk of harm and respond appropriately.

2.5. Robot-assisted monitoring of surgical procedure using biomimetic nociceptor

Encouraged by the above results, we decided to implement a pain reflex in a surgical robot with biomimetic nociceptor, thereby providing assistive tools to the surgeon (**Figure 5a**). In surgical procedures, the force exerted by the surgical robot needs to be appreciated visually according to the experience of surgical robot's operator.[26] The inability of the

This article is protected by copyright. All rights reserved.

15214095, ja, Downloaded from https://onlinelibrary.wiley.com/doi/10.1002/adma.202310555 by Wuhan University, Wiley Online Library on [01/12/2023]. See the Terms and Conditions (https://onlinelibrary.wiley.com/terms-and-conditions) on Wiley Online Library for rules of use; OA articles are governed by the applicable Creative Commons License

surgical robot to provide stimuli analysis and adaptive feedback could lead to instantaneous impact forces and potentially harmful mechanical stimuli that damage the patient. The possibility to recreate nociceptors in surgical robots could contribute to the future development of metaverse for intelligent healthcare via providing reference data.

Using a biopsy needle as a proof-of-concept model, the biomimetic nociceptor was integrated in the surgical robot and tested on various explanted biological tissues and organs (**Figure S41**). Statistically, the current measurements yielded different sensitivities associated with the tissues and organs, hence demonstrating the robot's ability to distinguish different tissues or organs during surgery (**Figure S42**). Additional experiments on animal models were carried out to validate the broad applicability of the biomimetic nociceptor to the surgical robot. Pain sensation and feedback of the biomimetic nociceptor were evaluated on various body positions in rat models, including muscle, rib, lung, heart and liver (**Figure 5b**). **Figure 5c** presents optical and electrical dual responses during biopsy procedures, enabling the spatial mapping of stimuli.

Figure 5d summarizes the results of currents obtained from various organs and tissues where mechanical stimuli were applied by the surgical robot. Measurement of force-induced currents yielded the highest results for rib, followed by muscle, whereas the results for heart,

This article is protected by copyright. All rights reserved.

Accepted Article

15214095, ja, Downloaded from https://onlinelibrary.wiley.com/doi/10.1002/adma.202310555 by Wuhan University, Wiley Online Library on [01/12/2023]. See the Terms and Conditions (https://onlinelibrary.wiley.com/terms-and-conditions) on Wiley Online Library for rules of use; OA articles are governed by the applicable Creative Commons License

Accepted Article

liver and lung yielded the lowest. The pain threshold value was preset based on above results, so that the protection program would stop the surgical robot if the signal reached a predefined current threshold. With increasing force exerted by the surgical robot, pain detection and pain reflex were more likely to appear for heart, liver and lung to avoid damaging the body (**Movie S6**). Pronounced mechanoluminescence was observed at the surgical site, and this assisted in achieving pain localization.

To simulate the application in robot-assisted surgery, a surgical procedure on a dog was monitored using our device (**Figure 5e** and **Figure S43**). The biomimetic nociceptor was mounted on a variety of tissues and organs in the dog to acquire electrical and optical signals, and the biopsy needle was applied to stimulate various locations across the dog. Images and signals associated with acquiring the current on various locations appear in **Figure 5f**. In agreement with the results from the rat, the sensitivity of current at soft-tissue locations can be greatly different from those at bony locations (**Figure 5g**). On the basis of statistical analyses of currents, we predefined the pain threshold value of each tissue or organ. The surgical robot was programmed to stop movement when the exerted force was above the pain threshold. During surgery, the surgical robot's pain sensing and reflex varied with position across the dog body (**Movie S7**). When the current exceeds the threshold for pain,

This article is protected by copyright. All rights reserved.

15214095, ja, Downloaded from https://onlinelibrary.wiley.com/doi/10.1002/adma.202310555 by Wuhan University, Wiley Online Library on [01/12/2023]. See the Terms and Conditions (https://onlinelibrary.wiley.com/terms-and-conditions) on Wiley Online Library for rules of use; OA articles are governed by the applicable Creative Commons License

protection program will activate the reflex movement to avoid damage to the tissues and organs. The above observations indicate that the biomimetic nociceptor enables the surgical robot to map the pain location and realize pain feedback, avoiding incorrect operation and damage at the surgical site. Future embodiments may incorporate further miniaturized biomimetic nociceptors mounted directly onto biopsy needles to afford pain perception and feedback in surgical procedures. After being integrated on a biopsy needle, the near-infrared mechanoluminescence of ZGGO:Cr may allow for *in vivo* pain localization with deep tissue penetration.

Accepted Article

This article is protected by copyright. All rights reserved.

15214095, ja, Downloaded from https://onlinelibrary.wiley.com/doi/10.1002/adma.202310555 by Wuhan University, Wiley Online Library on [01/12/2023]. See the Terms and Conditions (https://onlinelibrary.wiley.com/terms-and-conditions) on Wiley Online Library for rules of use; OA articles are governed by the applicable Creative Commons License

Accepted Article

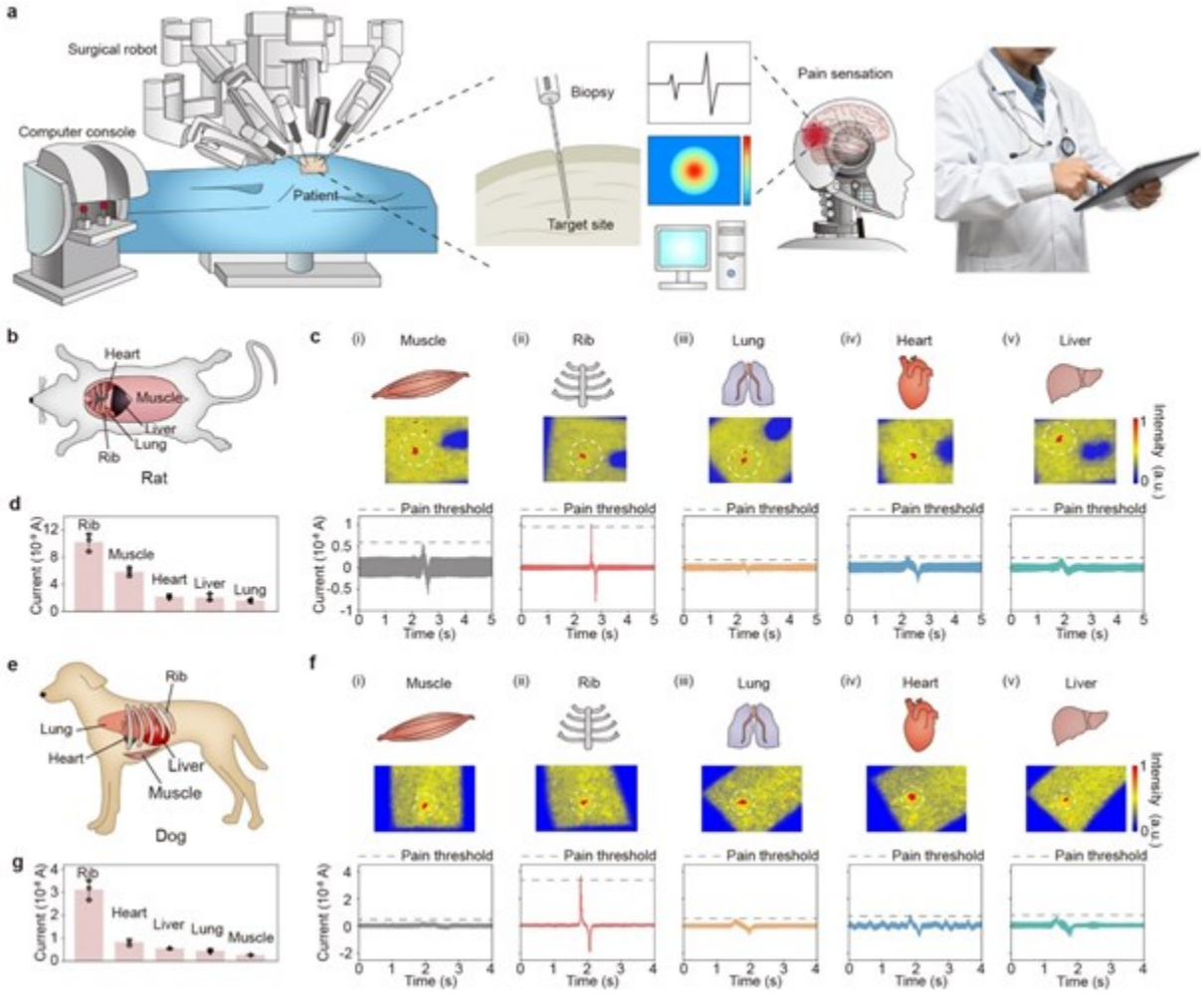

Figure 5. *Ex vivo* and *in vivo* demonstrations of robot-assisted biopsy surgery using biomimetic nociceptor. a) Overview of the robot-assisted biopsy surgery using biomimetic nociceptor to assist the surgeon to make surgery efficient. b) Schematic of surgery in the rat. c) Top: the mechanoluminescence images of device mounted on rat at different locations (muscle, rib, lung, heart and liver). The white dashed circles indicate the sites stimulated by

This article is protected by copyright. All rights reserved.

15214095, ja, Downloaded from https://onlinelibrary.wiley.com/doi/10.1002/adma.202310555 by Wuhan University, Wiley Online Library on [01/12/2023]. See the Terms and Conditions (https://onlinelibrary.wiley.com/terms-and-conditions) on Wiley Online Library for rules of use; OA articles are governed by the applicable Creative Commons License

Accepted Article

the surgical robot. The scale bar represents relative luminescence intensity. Bottom: the electrical signals generated when surgical robot exerts the same force on rat. Black dashed lines represent pain threshold. d) Statistics of peak generated current when surgical robot exerts the same force on rat. Data are mean ± s.d. n = 3. e) Schematic of surgery in the dog. f) Top: the mechanoluminescence images of device mounted on dog at different locations (muscle, rib, lung, heart and liver). White dashed circles indicate the sites that were stimulated by surgical robot. The scale bar represents relative luminescence intensity. Bottom: electrical signals generated when surgical robot exerts same force on dog. Black dashed lines represent pain threshold. g) Statistics of peak generated current when surgical robot exerts same force on dog. Data are mean ± s.d. n = 3.

3. Conclusion

In summary, we have developed a wireless biomimetic nociceptor with dual response pain sensory system, and implemented pain perception and pain reflex in intelligent terminals to mimic the complex characteristics of the body. Centrosymmetric ZGGO:Cr was found to exhibit synchronized optical and electrical responses under forces, offering an alternative approach to force-induced electricity without requiring non-centrosymmetric structures. The

This article is protected by copyright. All rights reserved.

15214095, ja, Downloaded from https://onlinelibrary.wiley.com/doi/10.1002/adma.202310555 by Wuhan University, Wiley Online Library on [01/12/2023]. See the Terms and Conditions (https://onlinelibrary.wiley.com/terms-and-conditions) on Wiley Online Library for rules of use; OA articles are governed by the applicable Creative Commons License

Accepted Article

integrated flexible unit with interactive program and wireless module forms a biomimetic nociceptor, supporting precise and rapid evaluation of pain threshold. To mimic the behavior of pain perception in the body, the biomimetic nociceptor benefited from machine-learning tools and implemented different pain thresholds in a robotic hand, allowing it to manipulate objects by applying precisely controlled forces while preventing damage to the robotic hand itself and the objects. Further, the results demonstrate the feasibility of biomimetic nociceptor in robot-assisted biopsy surgery, where implementation of this robotic system can provide feedback from different tissues or organs and assist the surgeon to make the procedure safer and more efficient. It is believed that such perception enables intelligent terminals to better respond to touch and pain in a manner akin to a human, potentially leading to more flexible, more productive and safer interactions with the surroundings and with humans. As a self-powered sensor, this triboelectric device may have potential to be deployed at scale in intelligent terminals. More broadly, with multi-function integration, this perception system will create opportunities across many scenarios, including smart devices, artificial intelligence, and Internet of Things.

4. Experimental Section

This article is protected by copyright. All rights reserved.

15214095, ja, Downloaded from https://onlinelibrary.wiley.com/doi/10.1002/adma.202310555 by Wuhan University, Wiley Online Library on [01/12/2023]. See the Terms and Conditions (https://onlinelibrary.wiley.com/terms-and-conditions) on Wiley Online Library for rules of use; OA articles are governed by the applicable Creative Commons License

Accepted Article

Preparation of ZGGO:Cr nanoparticles: $Zn_{1.2}Ga_{1.6}Ge_{0.2}O_4$: 0.5 % Cr (denoted as ZGGO:Cr) was synthesized according to previous method with slight modification.[27] ZGGO:Cr persistent luminescence nanoparticles were synthesized by hydrothermal method and high-temperature treatment. Firstly, GeO_2 (0.21 g, Aladdin) and NaOH (0.24 g, Sinopharm Chemical Reagent Co., Ltd.) were dissolved in ultrapure water (5 mL) and the solution was vigorously stirred to prepare Na_2GeO_3 precursor solution. Then $Zn(NO_3)_2{\cdot}6H_2O$ (2.1 g, Aladdin), $Ga(NO_3)_3{\cdot}9H_2O$ (4.0 g, Aladdin), $Cr(NO_3)_3{\cdot}9H_2O$ (0.01 g, Sinopharm Chemical Reagent Co., Ltd.) and as-prepared Na_2GeO_3 precursor solution (3 mL) were dissolved in ultrapure water (60 mL). $NH_3{\cdot}H_2O$ (28 wt % solution, Sinopharm Chemical Reagent Co., Ltd.) was slowly added to adjust the pH of mixed solution to about 8.5, followed by vigorous stir for 1 h. Next, the above colloidal suspension (pH 8.5) was transferred to the Teflon-lined stainless-steel autoclave for hydrothermal reaction at 220 °C for 12 h. Subsequently, the as-obtained ZGGO:Cr nanoparticles were collected by centrifugation and washed three times with ethanol. Dried ZGGO:Cr was ground into fine powder. Next, ZGGO:Cr was further heated at 1000 °C for 90 min, and was collected after cooling down to ambient temperature.

This article is protected by copyright. All rights reserved.

15214095, ja, Downloaded from https://onlinelibrary.wiley.com/doi/10.1002/adma.202310555 by Wuhan University, Wiley Online Library on [01/12/2023]. See the Terms and Conditions (https://onlinelibrary.wiley.com/terms-and-conditions) on Wiley Online Library for rules of use; OA articles are governed by the applicable Creative Commons License

Accepted Article

Morphology and structural characterization of ZGGO:Cr. Transmission electron microscope (TEM) (JEOL, JEM-2100) was used to characterize the morphology and size of ZGGO:Cr. X-ray diffraction (XRD) (JEOL, Miniflex600) was used to characterize the crystal structure.

Optical characterization of ZGGO:Cr. Persistent luminescence (PL) spectra were acquired by fluorescence spectrometer (Hitachi Co. Ltd., F-4600). Mechanoluminescence spectra were collected using a homemade mechanical setup and fluorescence spectrometer. Mechanoluminescence images of ZGGO:Cr were recorded using single lens reflex (SLR) camera (Nikon, D7200) and IVIS Lumina XR Imaging System (Caliper, Lumina XR) consisted of a charge coupled device (CCD) camera after illuminated with a portable ultraviolet (UV) lamp or sunlight.

Fabrication of pressure sensing unit. Two pieces of polyethylene glycol terephthalate (PET) films with the thickness of 0.5 mm were cut into squares with size of 1.5 cm × 1.5 cm, and Al film and Cu film were laminated on two PET films via double-sided adhesive respectively. To ensure the light transmission, the area of Al film was half that of PET film, so that the

This article is protected by copyright. All rights reserved.

15214095, ja, Downloaded from https://onlinelibrary.wiley.com/doi/10.1002/adma.202310555 by Wuhan University, Wiley Online Library on [01/12/2023]. See the Terms and Conditions (https://onlinelibrary.wiley.com/terms-and-conditions) on Wiley Online Library for rules of use; OA articles are governed by the applicable Creative Commons License

Accepted Article

ZGGO:Cr to be encapsulated between two films can be directly irradiated and observed from Al side. On the other hand, the area of Cu film was same as that of PET film to ensure electrical conductivity. The Cu wires were fixed in the edges of both Cu film and Al film. Thereafter, 0.1 g ZGGO:Cr nanoparticles were distributed evenly on the Cu film. Then, the side of Al film and PET film was pressed on ZGGO:Cr to cover the powders. Two pieces of PET films were sealed together with scotch tape carefully to avoid powder leakage. Finally, the pressure sensing unit based on ZGGO:Cr was fabricated after testing its electrical output and mechanoluminescence, which is described in detail below.

Linear mechano-sensing with electrical and optical response in pressure sensing unit. The pressure sensing unit was connected to electrochemical workstation (CH Instruments, CHI660d) and was fixed in the IVIS Lumina XR Imaging System keeping Al film at the top for light transmission. The pressure sensing unit was firstly pre-illuminated with 254 nm UV light or sunlight for 30 s. After the afterglow stabilized (that is, the PL intensity was attenuated at a ratio of 1% of the present luminescence intensity every 30 s), the exposure time was set to 0.5 s and the luminescence images of the pressure sensing unit were collected continuously. The PL background was obtained by two successive emission subtractions. Then, the

This article is protected by copyright. All rights reserved.

15214095, ja, Downloaded from https://onlinelibrary.wiley.com/doi/10.1002/adma.202310555 by Wuhan University, Wiley Online Library on [01/12/2023]. See the Terms and Conditions (https://onlinelibrary.wiley.com/terms-and-conditions) on Wiley Online Library for rules of use; OA articles are governed by the applicable Creative Commons License

Accepted Article

pressure sensing unit was pressed using different weights. The voltage signals were collected using electrochemical workstation. Simultaneously, the luminescence images of the pressure sensing unit were collected before and after the pressure was applied. According to the change of luminescence intensity after pressure with deducting the PL background, the mechanoluminescence intensity was obtained. All tests were repeated 3 times.

Fabrication of ZGGO:Cr@PDMS composite film: Firstly, polydimethylsiloxane (PDMS) precursor was prepared by mixing the base and curing agent of Sylgard 184 (Dow Corning) at 10:1 ratio in a culture dish. Then ZGGO:Cr nanoparticles were added, making sure that the mass ratio of PDMS and nanoparticles was 3:8. After stirring and mixing, above mixture was degasification in vacuum for 10 min and was cured at 85 °C for 2 h. Sample was taken out of the culture dish and was further cut into rectangular ZGGO:Cr@PDMS thin film. The stress-strain curves were obtained by universal testing machine. The surface potential of ZGGO:Cr@PDMS was measured by Kelvin probe force microscopy (KPFM) (Bruker, Dimension Icon).

This article is protected by copyright. All rights reserved.

15214095, ja, Downloaded from https://onlinelibrary.wiley.com/doi/10.1002/adma.202310555 by Wuhan University, Wiley Online Library on [01/12/2023]. See the Terms and Conditions (https://onlinelibrary.wiley.com/terms-and-conditions) on Wiley Online Library for rules of use; OA articles are governed by the applicable Creative Commons License

Accepted Article

Fabrication of wireless biomimetic nociceptor device: The device was composed of several different components. PDMS film at the top and polyimide (PI) film at the bottom were considered as transparent sealing layer and substrate, respectively. The innermost ZGGO:Cr@PDMS layer serves as triboelectric layer generating the triboelectric charge. This layer was encapsulated by Cu film and ITO film as electrodes. The electronic control module for signal process, wireless data transmission and power supply was connected to ITO and Cu via wires embedded in PDMS and PI. We fabricated and tested the devices of various sizes and shapes according to experimental requirements. The detailed procedures were described as following steps. (1) PI film as substrate was attached on a smooth silicon wafer. (2) Bottom Cu electrode with thickness of 100 nm was deposited on PI film by magnetron sputtering, and then the wire was connected to Cu electrode via Ag conductive epoxy. (3) ZGGO:Cr nanoparticles and PDMS precursor (ratio of base to curing agent is 10:1) were mixed at a mass ratio of 8:3. The mixture underwent fully stirring and mixing to form ZGGO:Cr@PDMS composite. (4) Above ZGGO:Cr@PDMS composite was spin-coated on the Cu-deposited PI substrate and was subsequently cured at 85 °C for 2 h. (5) ITO film with thickness of 70 nm was deposited on ZGGO:Cr@PDMS by magnetron sputtering. ITO film was connected to the wire via Ag conductive epoxy and was further sealed by spinning extra PDMS precursor. (6) Ultimately, the whole device was stripped from the silicon wafer and

This article is protected by copyright. All rights reserved.

15214095, ja, Downloaded from https://onlinelibrary.wiley.com/doi/10.1002/adma.202310555 by Wuhan University, Wiley Online Library on [01/12/2023]. See the Terms and Conditions (https://onlinelibrary.wiley.com/terms-and-conditions) on Wiley Online Library for rules of use; OA articles are governed by the applicable Creative Commons License

Accepted Article

was further connected to electronic control module, followed by subsequent characterization and test. After the fabrication of biomimetic nociceptor device, scanning electron microscopy (SEM) (Hitachi Co. Ltd., Regulus 8100) was used to characterize the structure and element mapping of the device.

Characterization of output electrical properties of the biomimetic nociceptor device: A homemade step motor was used to exert cyclical pressures on the biomimetic nociceptor device and the wireless data acquisition program was employed to record output current signals. Output signals under different frequency were acquired with different rotation speed. The biomimetic nociceptor device was pressed using different weights and linear current signals under varied pressure were collected wirelessly through computer. The readouts of commercial pressure sensor were regarded as a reference to calibrate the force. For the output signals under different mechanical stimuli, cotton swab, brush and needle were mounted on the homemade step motor and then the weights of 10 g, 20 g, 50 g, 100 g were hung in order, providing the biomimetic nociceptor device with continuous and increased friction force. The speed of applied force was adjusted by rotation speed and output current signals were recorded.

This article is protected by copyright. All rights reserved.

15214095, ja, Downloaded from https://onlinelibrary.wiley.com/doi/10.1002/adma.202310555 by Wuhan University, Wiley Online Library on [01/12/2023]. See the Terms and Conditions (https://onlinelibrary.wiley.com/terms-and-conditions) on Wiley Online Library for rules of use; OA articles are governed by the applicable Creative Commons License

Accepted Article

Spatially mapping of mechanical stimuli in the biomimetic nociceptor device: The biomimetic nociceptor device was pressed by different mechanical stimuli after pre-illumination by 254 nm UV light for 30 s, and the night vision camera was immediately used to obtain corresponding videos and images during the whole process. The images of mechanical stimuli localization were pseudo-colored with Image J software for the following analysis.

Statistical analysis: Results were presented as mean ± standard deviation (SD) from at least three independent experiments. The Student's t-tests in Supporting Information were performed by using Microsoft Excel to determine statistical significance between two groups. Image J software was used to analyze and process the mechanoluminescence images with pseudo-color. Python 3.6 software was used to analyze the results of dual responses and to define pain threshold.

Supporting Information

Supporting Information is available from the Wiley Online Library or from the author.

This article is protected by copyright. All rights reserved.

15214095, ja, Downloaded from https://onlinelibrary.wiley.com/doi/10.1002/adma.202310555 by Wuhan University, Wiley Online Library on [01/12/2023]. See the Terms and Conditions (https://onlinelibrary.wiley.com/terms-and-conditions) on Wiley Online Library for rules of use; OA articles are governed by the applicable Creative Commons License

Accepted Article

Acknowledgements

This work is supported by the National Natural Science Foundation of China (22174038, 21925401, 52221001), the Science and Technology Innovation Program of Hunan Province (2023RC3127), the Natural Science Foundation of Hunan Province (2022JJ20005), and the New Cornerstone Science Foundation through the XPLORER PRIZE. We thank Prof. Yu-Meng You at Southeast University, Nanjing, for his helpful suggestions for this work.

Conflict of Interest

The authors declare no conflict of interest.

Data Availability Statement

The data that support the findings of this study are available from the corresponding author upon reasonable request.

This article is protected by copyright. All rights reserved.

15214095, ja, Downloaded from https://onlinelibrary.wiley.com/doi/10.1002/adma.202310555 by Wuhan University, Wiley Online Library on [01/12/2023]. See the Terms and Conditions (https://onlinelibrary.wiley.com/terms-and-conditions) on Wiley Online Library for rules of use; OA articles are governed by the applicable Creative Commons License

Received: ((will be filled in by the editorial staff))

Revised: ((will be filled in by the editorial staff))

Published online: ((will be filled in by the editorial staff))

Accepted Article

References

[1] a) C. Peirs, R. P. Seal, *Science* **2016**, 354, 578; b) W. Wang, Y. Jiang, D. Zhong, Z. Zhang, S. Choudhury, J.-C. Lai, H. Gong, S. Niu, X. Yan, Y. Zheng, C.-C. Shih, R. Ning, Q. Lin, D. Li, Y.-H. Kim, J. Kim, Y.-X. Wang, C. Zhao, C. Xu, X. Ji, Y. Nishio, H. Lyu, J. B. H. Tok, Z. Bao, *Science* **2023**, 380, 735.

[2] D. W. Logan, *Dis. Model. Mech.* **2021**, 14, dmm049352.

[3] L. E. Osborn, A. Dragomir, J. L. Betthauser, C. L. Hunt, H. H. Nguyen, R. R. Kaliki, N. V. Thakor, *Sci. Robot.* **2018**, 3, eaat3818.

[4] a) L. Beaulieu-Laroche, M. Christin, A. Donoghue, F. Agosti, N. Yousefpour, H. Petitjean, A. Davidova, C. Stanton, U. Khan, C. Dietz, E. Faure, T. Fatima, A. MacPherson, S. Mouchbahani-Constance, D. G. Bisson, L. Haglund, J. A. Ouellet, L. S. Stone, J. Samson, M.-J. Smith, K. Ask, A. Ribeiro-da-Silva, R. Blunck, K. Poole, E. Bourinet, R. Sharif-Naeini,

This article is protected by copyright. All rights reserved.

15214095, ja, Downloaded from https://onlinelibrary.wiley.com/doi/10.1002/adma.202310555 by Wuhan University, Wiley Online Library on [01/12/2023]. See the Terms and Conditions (https://onlinelibrary.wiley.com/terms-and-conditions) on Wiley Online Library for rules of use; OA articles are governed by the applicable Creative Commons License

Cell **2020**, 180, 956; b) J. N. Wood, *Gut* **2004**, 53, ii9; c) J. H. Yoon, Z. Wang, K. M. Kim, H. Wu, V. Ravichandran, Q. Xia, C. S. Hwang, J. J. Yang, *Nat. Commun.* **2018**, 9, 417.

[5] a) M. Wang, Y. Luo, T. Wang, C. Wan, L. Pan, S. Pan, K. He, A. Neo, X. Chen, *Adv. Mater.* **2021**, 33, 2003014; b) A. Masteller, S. Sankar, H. B. Kim, K. Ding, X. Liu, A. H. All, *Ann. Biomed. Eng.* **2021**, 49, 57.

[6] a) S. Sundaram, *Science* **2020**, 370, 768; b) K. Yao, J. Zhou, Q. Huang, M. Wu, C. K. Yiu, J. Li, X. Huang, D. Li, J. Su, S. Hou, Y. Liu, Y. Huang, Z. Tian, J. Li, H. Li, R. Shi, B. Zhang, J. Zhu, T. H. Wong, H. Jia, Z. Gao, Y. Gao, Y. Zhou, W. Park, E. Song, M. Han, H. Zhang, J. Yu, L. Wang, W. J. Li, X. Yu, *Nat. Mach. Intell.* **2022**, 4, 893.

[7] a) S. J. Middleton, A. M. Barry, M. Comini, Y. Li, P. R. Ray, S. Shiers, A. C. Themistocleous, M. L. Uhelski, X. Yang, P. M. Dougherty, T. J. Price, D. L. Bennett, *Brain* **2021**, 144, 1312; b) S. Chun, J.-S. Kim, Y. Yoo, Y. Choi, S. J. Jung, D. Jang, G. Lee, K.-I. Song, K. S. Nam, I. Youn, D. Son, C. Pang, Y. Jeong, H. Jung, Y.-J. Kim, B.-D. Choi, J. Kim, S.-P. Kim, W. Park, S. Park, *Nat. Electron.* **2021**, 4, 429; c) M. Kumar, H.-S. Kim, J. Kim, *Adv. Mater.* **2019**, 31, 1900021; d) Y. Kim, Y. J. Kwon, D. E. Kwon, K. J. Yoon, J. H. Yoon, S. Yoo, H. J. Kim, T. H. Park, J.-W. Han, K. M. Kim, C. S. Hwang, *Adv. Mater.* **2018**, 30, 1704320.

This article is protected by copyright. All rights reserved.

Accepted Article

15214095, ja, Downloaded from https://onlinelibrary.wiley.com/doi/10.1002/adma.202310555 by Wuhan University, Wiley Online Library on [01/12/2023]. See the Terms and Conditions (https://onlinelibrary.wiley.com/terms-and-conditions) on Wiley Online Library for rules of use; OA articles are governed by the applicable Creative Commons License

Accepted Article

[8] a) F. Li, S. Gao, Y. Lu, W. Asghar, J. Cao, C. Hu, H. Yang, Y. Wu, S. Li, J. Shang, M. Liao, Y. Liu, R.-W. Li, *Adv. Sci.* **2021**, 8, 2004208; b) A. Chortos, J. Liu, Z. Bao, *Nat. Mater.* **2016**, 15, 937.

[9] Y. Dobashi, D. Yao, Y. Petel, T. N. Nguyen, M. S. Sarwar, Y. Thabet, C. L. W. Ng, E. Scabeni Glitz, G. T. M. Nguyen, C. Plesse, F. Vidal, C. A. Michal, J. D. W. Madden, *Science* **2022**, 376, 502.

[10] a) W. Wu, Z. L. Wang, *Nat. Rev. Mater.* **2016**, 1, 16031; b) T. Jiang, Y.-F. Zhu, J.-C. Zhang, J. Zhu, M. Zhang, J. Qiu, *Adv. Funct. Mater.* **2019**, 29, 1906068.

[11] J.-C. Zhang, X. Wang, G. Marriott, C.-N. Xu, *Prog. Mater. Sci.* **2019**, 103, 678.

[12] a) A. Biancoli, C. M. Fancher, J. L. Jones, D. Damjanovic, *Nat. Mater.* **2015**, 14, 224; b) D. S. Park, M. Hadad, L. M. Riemer, R. Ignatans, D. Spirito, V. Esposito, V. Tileli, N. Gauquelin, D. Chezganov, D. Jannis, J. Verbeeck, S. Gorfman, N. Pryds, P. Muralt, D. Damjanovic, *Science* **2022**, 375, 653.

[13] L. Wang, S. Liu, X. Feng, C. Zhang, L. Zhu, J. Zhai, Y. Qin, Z. L. Wang, *Nat. Nanotechnol.* **2020**, 15, 661.

This article is protected by copyright. All rights reserved.

15214095, ja, Downloaded from https://onlinelibrary.wiley.com/doi/10.1002/adma.202310555 by Wuhan University, Wiley Online Library on [01/12/2023]. See the Terms and Conditions (https://onlinelibrary.wiley.com/terms-and-conditions) on Wiley Online Library for rules of use; OA articles are governed by the applicable Creative Commons License

[14] a) Y. I. Sobolev, W. Adamkiewicz, M. Siek, B. A. Grzybowski, *Nat. Phys.* **2022**, 18, 1347; b) X. Qu, Z. Liu, P. Tan, C. Wang, Y. Liu, H. Feng, D. Luo, Z. Li, Z. L. Wang, *Sci. Adv.* **2022**, 8, eabq2521.

[15] a) X. Zheng, Y. Cheng, Y. Gao, T. Hu, J. Xu, H. Lin, Y. Wang, *J. Mater. Chem. C* **2023**, 11, 1747; b) H. Matsui, C.-N. Xu, Y. Liu, H. Tateyama, *Phys. Rev. B* **2004**, 69, 235109.

[16] a) C.-W. Woo, L. Schmidt, A. Krishnan, M. Jepma, M. Roy, M. A. Lindquist, L. Y. Atlas, T. D. Wager, *Nat. Commun.* **2017**, 8, 14211; b) P. Delmas, J. Hao, L. Rodat-Despoix, *Nat. Rev. Neurosci.* **2011**, 12, 139.

[17] a) X. Zhao, Z. Zhang, Q. Liao, X. Xun, F. Gao, L. Xu, Z. Kang, Y. Zhang, *Sci. Adv.* **2020**, 6, eaba4294; b) L. Li, L.-X. Cheng, L. Yang, J.-C. Zhang, *Macromol. Mater. Eng.* **2021**, 306, 2100017; c) L. Massari, G. Fransvea, J. D'Abbraccio, M. Filosa, G. Terruso, A. Aliperta, G. D'Alesio, M. Zaltieri, E. Schena, E. Palermo, E. Sinibaldi, C. M. Oddo, *Nat. Mach. Intell.* **2022**, 4, 425.

[18] B. Wang, Z. Chen, X. Li, J. Zhou, Q. Zeng, *J. Alloy. Compd.* **2020**, 812, 152119.

This article is protected by copyright. All rights reserved.

Accepted Article

15214095, ja, Downloaded from https://onlinelibrary.wiley.com/doi/10.1002/adma.202310555 by Wuhan University, Wiley Online Library on [01/12/2023]. See the Terms and Conditions (https://onlinelibrary.wiley.com/terms-and-conditions) on Wiley Online Library for rules of use; OA articles are governed by the applicable Creative Commons License

[19] a) Q. Ma, J. Wang, W. Zheng, Q. Wang, Z. Li, H. Cong, H. Liu, X. Chen, Q. Yuan, *Sci. China Chem.* **2018**, 61, 1624; b) C. Zhou, L. Peng, Z. Kong, M. Wu, M. S. Molokeev, Z. Zhou, J. Wang, M. Xia, *J. Mater. Chem. C* **2022**, 10, 5829.

[20] A. De Vos, K. Lejaeghere, D. E. P. Vanpoucke, J. J. Joos, P. F. Smet, K. Hemelsoet, *Inorg. Chem.* **2016**, 55, 2402.

[21] M. Szczot, J. Liljencrantz, N. Ghitani, A. Barik, R. Lam, J. H. Thompson, D. Bharucha-Goebel, D. Saade, A. Necaise, S. Donkervoort, A. R. Foley, T. Gordon, L. Case, M. C. Bushnell, C. G. Bönnemann, A. T. Chesler, *Sci. Transl. Med.* **2018**, 10, eaat9892.

[22] A. Szallasi, D. N. Cortright, C. A. Blum, S. R. Eid, *Nat. Rev. Drug Discov.* **2007**, 6, 357.

[23] K. L. Petersen, M. C. Rowbotham, *Neuroreport* **1999**, 10, 1511.

[24] M. Björnsdotter, I. Morrison, H. Olausson, *Exp. Brain Res.* **2010**, 207, 149.

[25] a) B. C. Kieseier, E. K. Mathey, C. Sommer, H.-P. Hartung, *Nat. Rev. Dis. Primers* **2018**, 4, 31; b) S. Boy, A. Reitz, A. Curt, B. Schurch, *Nat. Clin. Pract. Urol.* **2005**, 2, 199.

[26] A. Zemmar, A. M. Lozano, B. J. Nelson, *Nat. Mach. Intell.* **2020**, 2, 566.

This article is protected by copyright. All rights reserved.

Accepted Article

15214095, ja, Downloaded from https://onlinelibrary.wiley.com/doi/10.1002/adma.202310555 by Wuhan University, Wiley Online Library on [01/12/2023]. See the Terms and Conditions (https://onlinelibrary.wiley.com/terms-and-conditions) on Wiley Online Library for rules of use; OA articles are governed by the applicable Creative Commons License

[27] J. Wang, Q. Ma, X.-X. Hu, H. Liu, W. Zheng, X. Chen, Q. Yuan, W. Tan, *ACS Nano* **2017**, 11, 8010.

A biomimetic nociceptor with multi-dimensional mechano-sensing ability was demonstrated. Centrosymmetric crystal ZGGO:Cr exhibits strong force-induced electricity and luminescence output, with electrical signals quantitatively evaluating the pain level and the visual luminescence output providing pain site. This biomimetic nociceptor can be integrated with wireless communication module and intelligent analysis module to enable accurate recognition and feedback toward external harmful stimuli.

Wenjie Wang, Yingfei Wang, Li Xiang, Long Chen, Lilei Yu, Anlian Pan, Jie Tan*, and Quan Yuan*

A Biomimetic Nociceptor Using Centrosymmetric Crystals for Machine Intelligence

This article is protected by copyright. All rights reserved.

Accepted Article

15214095, ja, Downloaded from https://onlinelibrary.wiley.com/doi/10.1002/adma.202310555 by Wuhan University, Wiley Online Library on [01/12/2023]. See the Terms and Conditions (https://onlinelibrary.wiley.com/terms-and-conditions) on Wiley Online Library for rules of use; OA articles are governed by the applicable Creative Commons License

Accepted Article

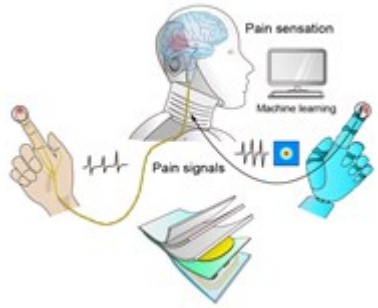

This article is protected by copyright. All rights reserved.

15214095, ja, Downloaded from https://onlinelibrary.wiley.com/doi/10.1002/adma.202310555 by Wuhan University, Wiley Online Library on [01/12/2023]. See the Terms and Conditions (https://onlinelibrary.wiley.com/terms-and-conditions) on Wiley Online Library for rules of use; OA articles are governed by the applicable Creative Commons License